Post-polymerization modification of poly(2-vinyl-4,4-dimethyl azlactone) as a versatile strategy for drug conjugation and stimuli-responsive release

Sk Arif Mohammad,[1] Veeresh B. Toragall,[1] Alex Fortenberry,[2] Oluwaseyi Shofolawe-Bakare,[2] Suresh Sulochana,[5] Katie Heath,[5] Iyanuoluwani Owolabi,[6] Garrett Tassin,[6] Alex S. Flynt,[6] Adam E. Smith,[1,2] Thomas Werfel[1,2,3,4]*

[1]Department of Biomedical Engineering, University of Mississippi, University, MS, 38677, USA

[2]Department of Chemical Engineering, University of Mississippi, University, MS, 38677, USA

[3]Department of BioMolecular Sciences, University of Mississippi, University, MS, 38677, USA

[4]Cancer Center and Research Institute, University of Mississippi Medical Center, Jackson, MS, 39216, USA

[5]Center of Biomedical Research Excellence in Natural Products Neuroscience, University of Mississippi, University, MS, 38677, USA

[6]Center for Molecular and Cellular Biosciences, University of Southern Mississippi, Hattiesburg, MS, 39406, USA

*Corresponding Author: E-mail: tawerfel@olemiss.edu (T. A. Werfel)

ABSTRACT

Post-polymerization modification of highly defined "scaffold" polymers is a promising approach for overcoming the existing limitations of controlled radical polymerization, such as batch-to-batch inconsistencies, accessibility to different monomers, and compatibility with harsh synthesis conditions. Using multiple physicochemical characterization techniques, we demonstrate that poly(2-vinyl-4,4-dimethyl azlactone) (PVDMA) scaffolds can be efficiently modified with a coumarin derivative, doxorubicin, and camptothecin small molecule drugs. Subsequently, we show that coumarin-modified PVDMA has high cellular biocompatibility and that coumarin derivatives are liberated from the polymer in the intracellular environment for cytosolic accumulation. In addition, we report the pharmacokinetics, biodistribution, and anti-tumor efficacy of a PVDMA-based polymer for the first time, demonstrating unique accumulation patterns based on the administration route (*i.e.,* intravenous vs. oral), efficient tumor uptake, and tumor growth inhibition in 4T1 orthotopic triple negative breast cancer (TNBC) xenografts. This work establishes the utility of PVDMA as a versatile chemical platform for producing polymer-drug conjugates with tunable, stimuli-responsive delivery.

Keywords: Stimuli-responsive polymers, post-polymerization modification, drug delivery, drug targeting and release

1. INTRODUCTION

Polymers having chemically responsive functional moieties are valuable tools for polymer scientists, adding to reactive/modular systems for developing various functional materials. While polymers with desirable functionalities can often be obtained by polymerizing vinyl-modified versions of the small-molecule active group,[1, 2] polymers having latent reactive moieties are valuable platforms for polymer scientists to develop functional materials with varying properties from a single scaffold, ensuring the daughter polymers retain the same degree of polymerization and polydispersity as the parent polymer. Such a methodology dramatically simplifies the identification of structure-property relationships that govern the behaviors of new materials.[3, 4] Azlactone (or oxazolone)-containing polymers are an effective platform for creating side-chain modified polymers and responsive surfaces and interfaces.[5, 6] Additionally, numerous molecule types, including proteins, peptides, and small molecules, can be used to functionalize these reactive scaffolds due to the stability of a wide range of azlactone-modified polymers in dimethyl sulfoxide, dimethyl formamide, and other organic solvents including methanol, n-heptanol, and benzyl alcohol.[7]

Many small molecule drugs (i.e., pharmaceutical agents) show poor bioavailability and insufficient pharmacokinetics because of their physicochemical characteristics, such as insolubility or lack of *in vivo* stability. The bioavailability of small molecule drugs depends on molecular flexibility, the polar surface area, and the total number of hydrogen bonds, which are often indirectly associated with the drug's molecular weight.[8] Polymeric drug delivery systems can improve the efficacy of these agents by making these drugs more water-soluble, extending their circulation time, enhancing the drug's localization in the target tissue, and limiting their exposure to healthy tissues.[9-11] Recently, the Chilkoti group reported drug-loaded nanoparticle synthesis via ring-opening polymerization (ROP) composed of a cyclic polymerizable group attached to pendant drug groups through a cleavable linker.[12] They used

poly(ethylene glycol) methyl ether (mPEG) as a macroinitiator for the synthesis of diblock copolymers of mPEG and drugamers (or drug-based monomers) that self-assemble into spherical micelles with a PEG corona. The same group reported paclitaxel-loaded drug nanoparticles via ROP,[13] and others have employed ROP for synthesizing biodegradable polypeptides,[14] polyesters,[15] polyphosphoesters,[16] and polycarbonates.[17] However, the direct polymerization of pharmaceutically active monomers is limited by the choice of available drug-based monomers, harsh synthesis conditions, and batch-to-batch variation in terms of polymer molecular weight and polydispersity.

Alternatively, platforms that allow large-scale synthesis of a single batch of polymer followed by post-polymerization modification would be highly desirable for ensuring consistency between batches and broadening the number of drugs that can be incorporated into macromolecular drug design. Poly(2-vinyl-4,4-dimethyl azlactone) (PVDMA) is one such polymer scaffold that could enable the precise macromolecular design of a wide range of polymer-based therapeutics. PVDMA offers a wide range of reactive flexibility and has been used for modification by a range of therapeutic compounds. In 2001, Heilmann et al. reported ring-opening modification of azlactones with alkyl and aryl nucleophiles, including primary amines, alcohols, and thiol functionalities.[18] The reactive azlactone functional group of PVDMA was utilized for controlled DNA release from thin films based on the charge-shifting of 2-dimethylaminoethanol(DMAE)-modified PVDMA.[19-24] Recently, the Moore group reported water-soluble protein-polymer conjugates through the functionalization of the azlactone ring with an amine-functionalized protein for improved intracellular delivery of the proteins.[25] Therefore, PVDMA could offer the ability to create a range of exciting polymer-drug conjugates with desirable properties such as broad chemical flexibility, optimizable structure/architecture, multivalent modifications, and highly tunable drug release. However, there are limited reports[26] on the functionalization of PVDMA with small molecule drugs, and

there has been no description of the *in vivo* bioavailability, pharmacokinetics, and biodistribution of PVDMA-based polymers to date.

In the present study, we report the cell trafficking, *in vivo* pharmacokinetics and anti-tumor efficacy of PVDMA-based stimuli-responsive materials. We employ reversible addition−fragmentation chain-transfer (RAFT) polymerization to synthesize well-defined, narrowly-dispersed PVDMA (**Scheme 1a**). We demonstrate that this strategy works for post-polymerization modification with a variety of structurally distinct drugs. Additionally, drug loading and release can be tuned by adjusting the ratio of the azlactone ring to the drug and creating linkages broken down by relevant *in vivo* triggers, such as pH and redox. Here, we use a PVDMA scaffold to produce representative delivery vehicles via post-polymerization modification (**Scheme 1**). We develop a strategy by which coumarin-based drugs can modify PVDMA following an alkylation reaction of the tertiary amine of DMAE with 3-bromoacetyl coumarin (DBAC; **Scheme 1b**). Additionally, we show that PVDMA can be modified with the chemotherapeutic drugs doxorubicin (**Scheme 1c**) and camptothecin (**Scheme 1d**) to demonstrate the broad applicability of this approach. The potential of the formulated polymer-drug conjugates is assessed by determining the *in vitro* release kinetics, cellular uptake, and cytotoxicity in tumor and kidney cell lines. Further, we study the *in vivo* pharmacokinetics, biodistribution, and anti-tumor efficacy of DBAC-modified PVDMA polymers in mice, representing the evaluation of PVDMA-based polymers *in vivo* for the first time.

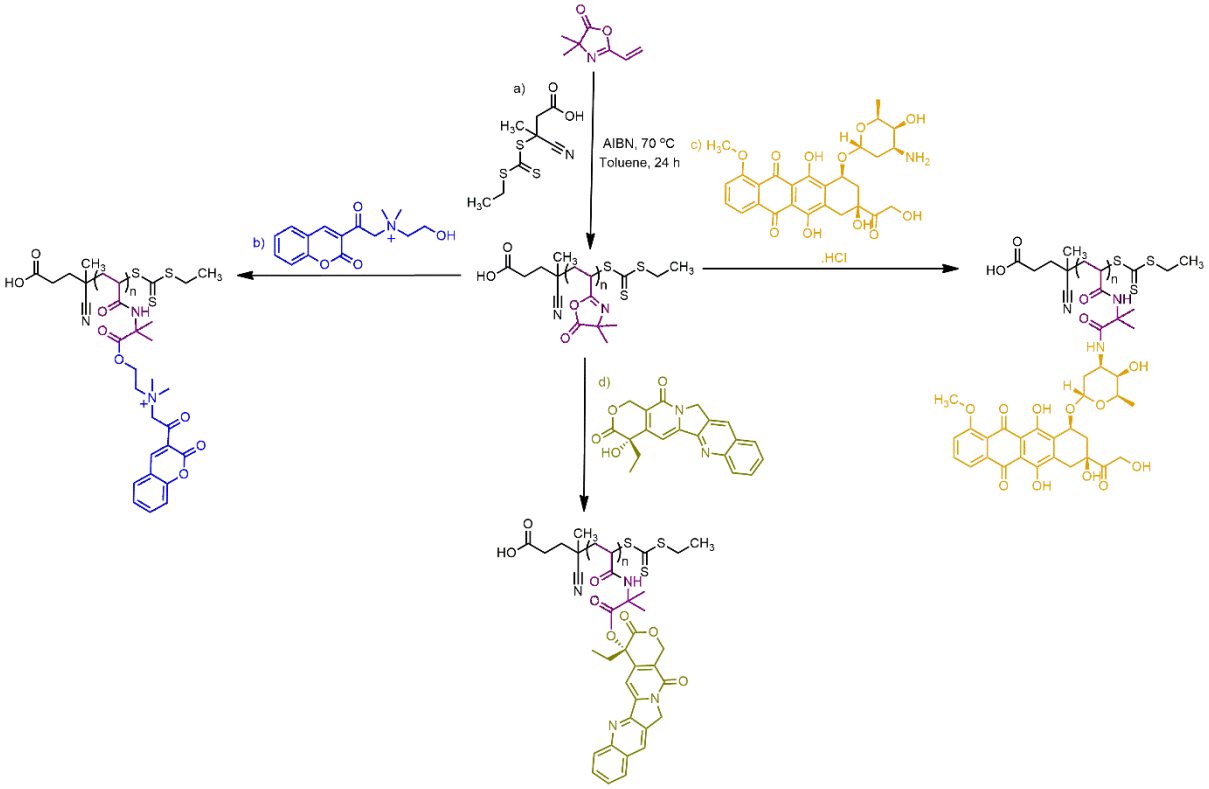

Scheme 1: Synthetic pathways for a) the PVDMA polymer scaffold, b) Post-polymerization modification of the PVDMA scaffold by DBAC, c) Post-polymerization modification of PVDMA by doxorubicin, and d) Post-polymerization modification of PVDMA by camptothecin.

2. EXPERIMENTAL SECTION

2.1. Materials

All materials were used as received without further purification unless noted otherwise. Vinyl azlactone (VDMA) purchased from Polysciences, USA. RAFT agent 4-Cyano-4-(((ethylthio)carbonothioyl)thio)pentanoic acid (ECT) and initiator 2,2′-Azobis(2-methylpropionitrile) (AIBN), 3-bromoacetyl coumarin (BAC), 2-Dimethylaminoethanol (DMAE), 1,8-diazabicyclo[5.4.0]-undec-7-ene (DBU), 4-Aminophenyl disulfide (APD), L-Glutathione reduced (GSH), Triethylamine (TEA), Potassium phosphate monobasic, Potassium phosphate dibasic, Trizma Base, and Trizma HCl were purchased from Sigma-Aldrich, USA. Tetramethylrhodamine Cadaverine (TMR) and Phosphate-Buffered Saline (pH

7.4) were purchased from ThermoFisher Scientific, USA. Dialysis bag MW cut off 3.5 KDa was purchased from Fisher Scientific, USA. Doxorubicin Hydrochloride was purchased from TCI Chemical, USA. Camptothecin was procured from Selleck Chemicals. Chloroform-d ($CDCl_3$), Methanol-d4, deuterium oxide (D_2O), N,N-Dimethylsulfoxide-d_6 were purchased from Sigma-Aldrich, USA. Toluene, acetone, diethyl ether, N,N-dimethylformamide (DMF), dimethyl sulfoxide (DMSO), methanol, and acetonitrile were purchased from Fisher Chemicals, USA.

2.2. Methods

2.2.1. Homopolymerization of (2-vinyl-4,4-dimethyl azlactone) via reversible addition-fragmentation chain transfer (RAFT) polymerization

The reaction was performed in a single-neck pear-shaped 50 mL round-bottom reaction flask equipped with a Teflon-coated magnetic stir bar. VDMA monomer (8.0 g, 57.5 mmol), ECT (84.3 mg, 0.32 mmol), AIBN (5.25 mg, 0.032 mmol), and toluene (24 mL) were added into the round-bottom flask. The round-bottom flask was sealed with a rubber septum and purged with nitrogen for 30 minutes. The reaction mixture was placed in a preheated oil bath at 70 °C for 24 h. Finally, the reaction was quenched by placing a round-bottom flask into an ice bath. The product was isolated by two precipitations in chilled cold diethyl ether and dried in vacuo. ^{1}H NMR (400 MHz, $CDCl_3$, δ in ppm): 1.55-1.30 (O=C-C-(C<u>H</u>$_3$)$_2$ and -CH_2-C<u>H</u>$_3$ signal a), 2.18-1.82 (-C<u>H</u>$_2$CH, signal d), 2.84-2.60 (-CH_2C<u>H</u>, signal C). FTIR (ATR, cm^{-1}): 2975 (4,4-dimethyl groups on the azlactone ring), 2933 and 2867 (C-H str. of methylene and methine backbone signals), 1810 (lactone C=O) and 1668 (C=N).

2.2.2. Synthesis of N-(2-hydroxyethyl)-N,N-dimethyl-2-oxo-2-(2-oxo-2H-chromen-3-yl)ethanaminium (DBAC)

The DBAC was synthesized by following a previously reported procedure.[27] 3-bromoacetyl coumarin (0.5 g, 1.87 mmol) and 2-dimethylaminoethanol (2.0 mL, 19.87 mmol) were taken in a 15-ml pear-shaped flask and vortexed vigorously. After that, the reaction vessel was placed in a preheated oil bath at 40 °C and stirred for 2 hours. The reaction mixture was allowed to cool to room temperature, then added dropwise into acetone (this process was done three times), and a brown precipitate was obtained. The precipitate was collected by filtration and dried under vacuum. ^{1}H NMR (400 MHz, D_2O, δ in ppm): 2.83-2.73 (-CH_2-O<u>H</u>, signal a), 3.51-3.42 and 3.22-3.13 (-CH_2-N($C\underline{H}_3$)$_2$, signal d and e), 3.62-3.53 (-N-$C\underline{H}_2$-CH_2, signal c), 4.19-3.73 (-CH_2-$C\underline{H}_2$-OH, signal b), 4.64-4.46 (O=C-$C\underline{H}_2$. signal f), 7.42-7.28 (-C<u>H</u> of benzene, signal i), 7.74-7.54 (-C<u>H</u> of benzene, signal h), 8.38-8.25 (O=C-C=C<u>H</u>, signal g). FTIR (ATR, cm^{-1}): 3125, 3031, and 3014 (C–H vibrations of 3-bromoacetyl coumarin), 1716 (C=O stretching frequency of 3-bromoacetyl coumarin), 1606 and 1577 (ring vibration which is localized on the benzene part of the molecule), 3395 (OH stretching of DMAE).

2.2.3. Post-polymerization modification of PVDMA by DBAC

The five-member ring of PVDMA was opened by the following procedure: in a 15-ml pear-shaped flask, PVDMA (150 mg, 1.07 mmol with respect to monomer repeat unit) was taken and dissolved in 2 ml of DMF. DBAC (595 mg, 2.154 mmol) was separately dissolved in 5 ml of DMF in another vial. After the solutions were mixed, DBU (323 µl, 2.154 mmol) was added. The reaction was allowed to run for 24 hours at 50 °C. The product was subsequently precipitated in chilled diethyl ether (the precipitation process was done three times). The precipitate was collected by filtration and dried under vacuum. ^{1}H NMR (400 MHz, MeOD, δ in ppm): 1.60-1.50 (-NH-C($C\underline{H}_3$)$_2$, CN-C-$C\underline{H}_3$ and -CH_2-$C\underline{H}_3$, signal a, b and c), 2.46-2.12 (-

C$\underline{H}_2$CH and COOH-C$\underline{H}_2$, signal d and e), 3.59 and 3.27 (-CH2-N(C$\underline{H}_3$)$_2$, signal f and g), 3.37 (-CH$_2$-C$\underline{H}$, signal h), 3.64-3.63 (-O-CH$_2$-C$\underline{H}_2$, signal i), 4.77-4.57 (-N-C$\underline{H}_2$-C=O, signal j), 4.26-4.12 (-O-C$\underline{H}_2$-C$\underline{H}_2$, signal k), 7.47-7.34 (-C$\underline{H}$ of benzene, signal n), 7.77-7.66 (-C$\underline{H}$ of benzene, signal m), 8.04-7.89 (-C=O-N$\underline{H}$, signal o), 8.37-8.31 (-C$\underline{H}$-C-C=O, signal l). FTIR (ATR, cm^{-1}): 1714 (C=O stretching frequency of ester), 1646 (C=O stretching of amide), 1535 (N-H bending of amide), 2975 (4,4-dimethyl groups on the azlactone ring), 2933 and 2867 (C-H str. of methylene and methine backbone signals), 3300 (N-H stretching of amide).

2.2.4. Post-polymerization modification of PVDMA by anti-cancer drugs

PVDMA polymer (50 mg, 0.36 mmol) and doxorubicin-HCl (53 mg, 0.09 mmol) were taken in a 10 ml pear-shaped flask and dissolved in 1.5 mL DMF solvent. Further, triethylamine (TEA) (13 µL, 0.09 mmol) was added to the mixture and then continued stirring at room temperature for 24 h under dark conditions. After that, the doxorubicin-modified PVDMA polymer was purified by dialysis against DMF, and then water with a 3.5 KDa molecular weight cut off dialysis bag. The recovered sample was then frozen and lyophilized. ^{1}H NMR (400 MHz, DMSO-d6, δ in ppm): 1.48-1.11 (-NH-C(C$\underline{H}_3$)$_2$, -CH$_2$-C$\underline{H}_3$, and -O- CH$_2$-C$\underline{H}_3$, signal a, b and c), 1.92-1.77 (-CH-C$\underline{H}_2$, signal d), 2.34-2.15 -CH-C$\underline{H}_2$, signal e), 3.13-2.99 (-C-C$\underline{H}_2$-C, signal f), 4.05-3.88 (-O-C$\underline{H}_3$, signal i), 4.28-4.10 (-O-C$\underline{H}$-CH$_3$, signal j), 4.71-4.48 (-C=O-C$\underline{H}_2$-OH, signal k), 5.07-4.76 (-CH$_2$-C$\underline{H}$-O-, signal g), 5.54-5.13 (-O-C$\underline{H}$-CH$_2$, signal h), 6.41-6.01 (-O$\underline{H}$ of doxorubicin), 7.82-7.33 (benzene ring of doxorubicin), 8.23-7.87 (-N$\underline{H}$ of amide and doxorubicin), 14.18-13.84 and 13.41-13.07 (-Ar-O$\underline{H}$ of doxorubicin). FTIR (ATR, cm^{-1}): 1720 (C=O stretching frequency of doxorubicin), 1652 (C=O stretching of amide), 1533 (N-H bending of amide), 1411 (doxorubicin str.), 1284 (doxorubicin str.), 1016 and 985 (doxorubicin str.), 792 and 763 (doxorubicin str.).

PVDMA polymer (50 mg, 0.36 mmol) and camptothecin (125.5 mg, 0.36 mmol) were taken in a 10 ml pear-shaped flask and dispersed in 5 mL DMF solvent. Further, DBU (54 µL, 0.36 mmol) was added to the mixture and purged with nitrogen for 30 minutes. Next, the reaction mixture was placed into a preheated 40 °C oil bath with stirring for 24 h. After that, camptothecin-modified PVDMA polymer was purified by dialysis against DMF and then water with a 3.5 KDa cut off dialysis bag. The recovered sample was then frozen and lyophilized. ^{1}H NMR (400 MHz, DMSO-d6, δ in ppm): 0.94-0.83 (-C-CH_2-C$\underline{H}_3$, signal a), 1.74-1.12 (-NH-C(C$\underline{H}_3$)$_2$, -CH_2-C$\underline{H}_3$, and -CH_2-C-C$\underline{H}_3$, signal b, c and d), 2.38-1.97 (-C-C$\underline{H}_2$-CH_3, signal e), 2.77-2.62 (-CH_2-C$\underline{H}$, signal f), 3.29-3.21 (-C$\underline{H}_2$-CH_3, signal g), 5.35-5.16 (-C=O-N-C$\underline{H}_2$, signal i), 5.51-5.37 (-C=C$\underline{H}$, signal j), 6.67-6.45 (camptothecine), 7.39-7.34 (-C=C$\underline{H}$, signal h), 8.24-7.63 and 8.77-8.55 (benzene ring of camptothecine). FTIR (ATR, cm^{-1}): 1735 (C=O stretching frequency of ester), 1579 and 1155 (camptothecine str.).

2.2.5. In vitro drug release studies

DBAC release studies were carried out in different pH (5.5 and 7.4) 0.3 M buffer solutions. DBAC-modified PVDMA polymer (5 mg) was dissolved in 1 ml buffer solution and poured into a 3.5 kDa MW cut off dialysis bag. At 37 °C, we performed dialysis against a 100 ml volume buffer solution. Over time, supernatants were gathered from the buffer solution and measured via UV-VIS spectrophotometry. Absorbance was measured at 316 nm for a wide range of concentrations of DBAC, including 0.005, 0.010, 0.015, 0.020, 0.025, 0.030 and 0.035 mg/ml. Absorbance readings at 316 nm were used to generate a linear standard curve of absorbance vs. concentration.

2.2.6. Cell culture

Cancer cells (HeLa) and human embryonic kidney cells (HEK-293) (ATCC, USA) were cultured in EMEM (Corning, USA) and DMEM (Gibco) media, respectively, each containing 10% FBS (Gibco) and 1% Anti-Anti (100X) reagent (Gibco). All cell lines were maintained at 37 °C and 5% CO_2.

2.2.7. Cell viability

HeLa and HEK-293 cells in culture media were seeded in three replicates in a 96-well plate at a density of 3,000 cells/well. The cells were allowed to adhere and proliferate for 24 hr before replacing the media with new media containing varying concentrations of polymer solution (0-1000 μg/mL). The cells were incubated with the new media for 24 hr, after which the CellTiter Glo™ (Promega, Cat. No. G9242) assay was performed, and the luminescence of the cells was measured on a microplate reader (BioTek Synergy H1).

2.2.8. Synthesis of both DBAC and tetramethyl rhodamine (TMR) cadaverine-modified PVDMA polymer

The synthesis of fluorescently-labeled derivatives of PVDMA was performed by slight modification of a previous report.[28] PVDMA (150 mg, 1.078 mmol w.r.t monomer repeat unit), DBAC (296 mg, 1.07 mmol), and DBU (162 μl, 1.078 mmol) were taken into a 10 mL round-bottomed flask and dissolved in 4 mL of DMSO. In a separate vial, TMR (2.77 mg, 0.005 mmol) was dissolved in 1 mL DMSO and transferred into the mixture in the round-bottom flask. The flask was capped with a septum and stirred in the dark at 50 °C for 24 h. The solution was precipitated dropwise into 20 mL of cold diethyl ether, filtered, and dried under vacuum. ^{1}H NMR (400 MHz, DMSO-d6, δ in ppm): 1.55-1.18 (-NH-C(C$\underline{H}_3$)$_2$, signal a), 2.78-2.73 (-$CH_2C\underline{H}$, signal b), 3.49 and 3.21 (-C-N(C$\underline{H}_3$)$_2$, signal c and d), 3.57 (-O-CH_2-C$\underline{H}_2$, signal e),

4.64-4.31 (-O-CH_2-CH2, signal f), 4.19-4.06 (-N-C<u>H</u>$_2$-C=O, signal g), 7.58-7.17 (-C<u>H</u> of benzene and TMR, signal h), 7.75-7.59 (-C<u>H</u> of benzene, signal i), 7.97-7.86 (TMR), 8.33-8.25 (-C=O-C=C<u>H</u>, signal j). FTIR (ATR, cm^{-1}): 1714 (C=O stretching frequency of ester), 1646 (C=O stretching of amide), 1535 (N-H bending of amide), 2975 (4,4-dimethyl groups on the azlactone ring), 2933 and 2867 (C-H str. of methylene and methine backbone signals), 3300 (N-H stretching of amide), 701 (benzene derivative).

2.2.9. Measurement of fluorescently-labeled PVDMA at various concentrations

For making a standard curve of TMR-modified polymer fluorescence, we measured the fluorescence intensity of DBAC-TMR-PVDMA using a microplate reader (BioTeK synergy H1) at an excitation wavelength of 544 nm and emission wavelengths of 575 nm. We started the measurement of TMR- and DBAC-modified PVDMA polymers in various concentrations ranging from 3.7 mg/mL to 0.0003 mg/mL by dissolving them in a pH 7.4 PBS buffer.

2.2.10. Intracellular trafficking of DBAC-TMR-PVDMA imaged via confocal microscopy

HEK-293 cells were utilized for intracellular imaging. The cells were grown under standard conditions (37°C, 5% CO_2, DMEM media with 10% FBS) in glass bottom culture vessels. 10 μg ml^{-1} of DBAC-TMR-PVDMA polymer was added to the cells and incubated for 10 minutes or ON, after which fluorescence associated with dyes was imaged. In addition, time lapse imaging of dye distribution in cells was taken for 3 hours after adding 100 μg ml^{-1} of the dye to cells in glass bottom culture vessels.

2.2.11. Subcellular colocalization imaging of DBAC-TMR-PVDMA

HEK-293 cells were grown under standard conditions (37°C, 5% CO2, DMEM media with 10% FBS) in glass bottom culture vessels. Imaging of DBAC-TMR-PVDMA distribution in

cells was done after a 2 h incubation with 50 μg ml^{-1} of DBAC-TMR-PVDMA polymer in cell culture media. Cells were co-stained with LysoTracker Green DND-26 (Invitrogen) 10 mins before imaging and washed with 1 ml PBS. Fluorescence and colocalization of dyes were visualized and measured with a Leica Stellaris STED confocal microscope.

2.2.12. Pharmacokinetics of DBAC-TMR-PVDMA

All procedures were performed in compliance with the University of Mississippi Animal Care and Use Committee and following the National Institutes of Health (NIH) guidelines. Male and female CD-1 mice (50:50 male: female ratio) were quarantined in the University of Mississippi's animal house for 7 days with a 12 h dark/light cycle. During this period, they had free access to standard pellet feed and water. Either DBAC or DBAC-TMR-PVDMA were administered at 10 mg/kg through oral gavage or retro-orbital IV injection at a volume of 0.1 mL. The vehicle for DBAC was 10% absolute alcohol, 10% cremophor and 80% Milli-Q water, whereas the DBAC-TMR-PVDMA polymer was administered in 100% PBS. At different times post-injection (0.5, 1, 3, 6, 8 and 15 h for oral and 0.12, 0.25, 0.5, 1, 3, and 8 h for IV) mice were induced with 5% isoflurane and maintained with 2% isoflurane (Covetrus, #029405). Blood was collected by cardiac puncture and stored in K2 EDTA tubes (SAI Infusion Technologies, #MVCB-E-300). Mice were then perfused through the heart with PBS (Life Technologies, #10-010-072). Plasma was harvested by centrifuging the blood using Eppendorf 5430R Centrifuge (Germany) at 5,000 rpm for 5 min and stored frozen at -80 ± 10°C until analysis. Following the collection of GI tract, heart, lung, spleen, liver, or kidney tissues in a separate 15 mL round-bottom screw-capped vial, phosphate-buffered saline (5 volumes of each tissue) was added and homogenated with a homogenizer (Polytron®) and stored at -80 ± 10°C until analysis.

2.2.13. Sample preparation for DBAC detection

A simple protein precipitation method was followed to extract DBAC from mice plasma. To an aliquot of 50 µL of plasma or tissue (GI tract, heart, lung, spleen, liver, or kidney) samples, tolbutamide (internal standard, IS) solution (5 µL of 20 ng/mL) was added and mixed for 15 s on a cyclomixer (Thermo Scientific, IN, USA). After precipitation with 500 µL of acetonitrile, the mixture was vortexed for 2 min, followed by centrifugation for 10 min at 14,000 rpm on an accuSpin Micro 17R (Fisher Scientific, USA) at 5 ℃. An aliquot of ~150 µL of clear supernatant was transferred into vials, and 2 µL was injected into the UPLC-MS/MS system for analysis. The primary stock solutions of DBAC and tolbutamide (IS) were prepared in methanol at 1.0 mg/ml concentration. Working solutions of calibration standards and quality control (QC) samples were prepared by dilution with methanol and stored at -20°C. A working stock of the IS solution (20 ng/mL) was prepared in methanol and stored at -20°C.

2.2.14. Sample preparation for fluorescence detection of DBAC-TMR-PVDMA in plasma and other tissues

We took 0.1 mL aliquot of all tissues (GI tract, Liver, Heart, Kidney, Spleen, and Lungs) except Plasma (20 uL added in 40 uL pH 7.4 PBS buffer) for measuring the fluorescence intensity of DBAC-TMR-PVDMA polymer. We used a microplate reader (BioTeK synergy H1) to measure the fluorescence intensity at an excitation wavelength of 544 nm and emission wavelengths of 575 nm. We calculated the concentration of fluorescently labeled polymer in plasma and other tissues based on the standard curve in **Figure S10**.

2.2.15. Biocompatibility of DBAC-TMR-PVDMA after intravenous administration

CD-1 mice (4-6 weeks of age; 50:50 M:F) were injected intravenously via the tail vein with DBAC-PVDMA (10 mg/kg and 33.3 mg/kg) or PBS at a volume of 100 µL per injection. Mice

were rested from treatment and weighed twice per week until sacrifice at 14 days post-injection. At the time of sacrifice, blood was collected by cardiac puncture, and major organs were collected, weighed, and fixed in 10% formalin. Hematological parameters were analysed using the automated Sysmex XT-V (IL, USA) hematolyser. The whole blood was collected in EDTA-coated tubes at the end of each experiment was analyzed for erythrocyte count (RBC), white blood cells (WBC), hemoglobin (HGB), and other hematology parameters. The serum was separated from whole blood by clotting at room temperature and followed by centrifugation at 1500×g for 10 min. The serum was used to evaluvate the clinical chemistry parameters (ALT, AST, BUN, ALP, etc.) analyzed using the AU680 clinical chemistry analyzer (Beckman Coulter, California, USA). For histopathology analysis, organs (liver, heart, and kidney) were processed for paraffin embedding, stained with hematoxylin and eosin, and examined microscopically for histological changes.[29]

2.2.16. Tumor targeting and anti-tumor efficacy of DBAC-TMR-PVDMA

Balb/C mice (4-6 weeks of age; 0:100 M:F) were injected in the 4th inguinal mammary fatpad with 1e6 4T1 tumor cells in a 100 μL solution of Matrigel and PBS (50:50). Mice were observed daily once palpable tumors were observed. Once tumors reached 100 mm^3, mice were administered DBAC-TMR-PVDMA (10 mg/kg, *i.v.*), DBAC (equivalent dose, *i.v.*), or PBS once per week via tail vein injection. Tumor growth was monitored by caliper measurement every three days until the study endpoint, and tumor volume was calculated as 0.5 x length x width^2). Mice were sacrificed 21 days following the first treatment administration, followed by collection, weighing, and fixation of tumors and major organs in 10% formalin.

2.2.17. Stastical analysis

The data are represented as mean ± SD. Significance between groups interpreted by student T test and one way ANOVA with Post Tukeys test, where $P \leq 0.05$ is considered as significantly different using graph pad Prism (v. 10.1.1).

3. RESULTS AND DISCUSSION

3.1. Synthesis of PVDMA homopolymer and DMAE-modified 3-bromoacetyl coumarin (DBAC)

We utilized RAFT polymerization to synthesize well-defined and narrowly dispersed PVDMA homopolymers of three molecular weights (**Scheme 1a** and **Figure S1**). The structural characterization of PVDMA homopolymers was confirmed by ^{1}H-NMR (**Figure S1a**) and FTIR spectroscopy (**Figure S1b**). In the ^{1}H NMR spectra, we identified azlactone ring-associated methyl groups at the peak at 1.55-1.30 ppm, while the peaks at 2.18 and 2.84 correspond to the polymer backbone. Moreover, FTIR spectroscopy revealed C=O stretching at 1810 cm^{-1} and C=N stretching at 1668 cm^{-1} of the azlactone ring. Gel permeation chromatography (GPC) results verified that PVDMA could be synthesized with varying molecular weights (P1 = 10,440 Da, P2 = 15,460 Da, and P3 = 23,180 Da) and consistently produce polymers of low polydispersity (P1 = 1.03, P2 = 1.01, and P3 = 1.03) (**Figure S1c-e, Table S1**).

3.2. Functionalization of PVDMA polymer with drug molecules

Next, DBAC was produced by a tertiary amine alkylation reaction between BAC and DMAE (**Scheme S1**), followed by confirmation by ^{1}H-NMR (**Figure S2**) and FTIR spectroscopy (**Figure S3**).[30, 31] PVDMA (P3) was subjected to post-polymerization modification by DBAC (**Scheme 1b**), followed by ^{1}H-NMR and FTIR spectroscopy to confirm the conjugation

reaction. ^{1}H-NMR confirms the successful functionalization of the azlactone ring of PVDMA polymer by DBAC (**Figure 1a**). In the ^{1}H-NMR spectra, the peak at 2.46-2.12 ppm corresponds to the polymer backbone, the peaks at 3.59 and 3.27 ppm indicated the presence of the DMAE-associated methyl groups, while peaks at 7.47-7.34, 7.77-7.66, and 8.04-7.89 ppm revealed aromatic ring protons of coumarin. Utilizing FTIR (**Figure 1b**), we observed the disappearance of the peak at 1810 cm^{-1} for the C=O stretching frequency of the azlactone ring and a sharp, new peak at 1714 cm^{-1} for the C=O stretching frequency of ester moieties, in addition to a peak at 2975 cm^{-1} revealing the C-H stretching frequency of the methyl group of the azlactone ring indicating the complete opening of the azlactone ring of PVDMA and substitution by DBAC.[32] To exemplify the versatile nature of PVDMA as a scaffold for post-polymerization modification by a range of compounds, we also modified PVDMA with the anti-cancer drugs doxorubicin and camptothecin (**Scheme 1c-d**). Doxorubicin-modified PVDMA was structurally characterized by ^{1}H-NMR (**Figure 1c**) and FTIR spectroscopy (**Figure 1d**). ^{1}H-NMR spectroscopy of doxorubicin-modified PVDMA polymer revealed a number of doxorubicin-associated peaks in the final conjugate, including aromatic carbon protons, aromatic ring-associated hydroxyl protons, and others. FTIR spectroscopy exhibited a peak at 1720 cm^{-1}, indicating C=O stretching frequency of doxorubicin, and the peaks at 1652 and 1533 cm^{-1} for C=O stretching and N-H bending of amide, respectively. ^{1}H-NMR (**Figure S4**) and FTIR spectroscopy (**Figure S5**) also demonstrated the successful modification of the PVDMA scaffold by the camptothecin drug.

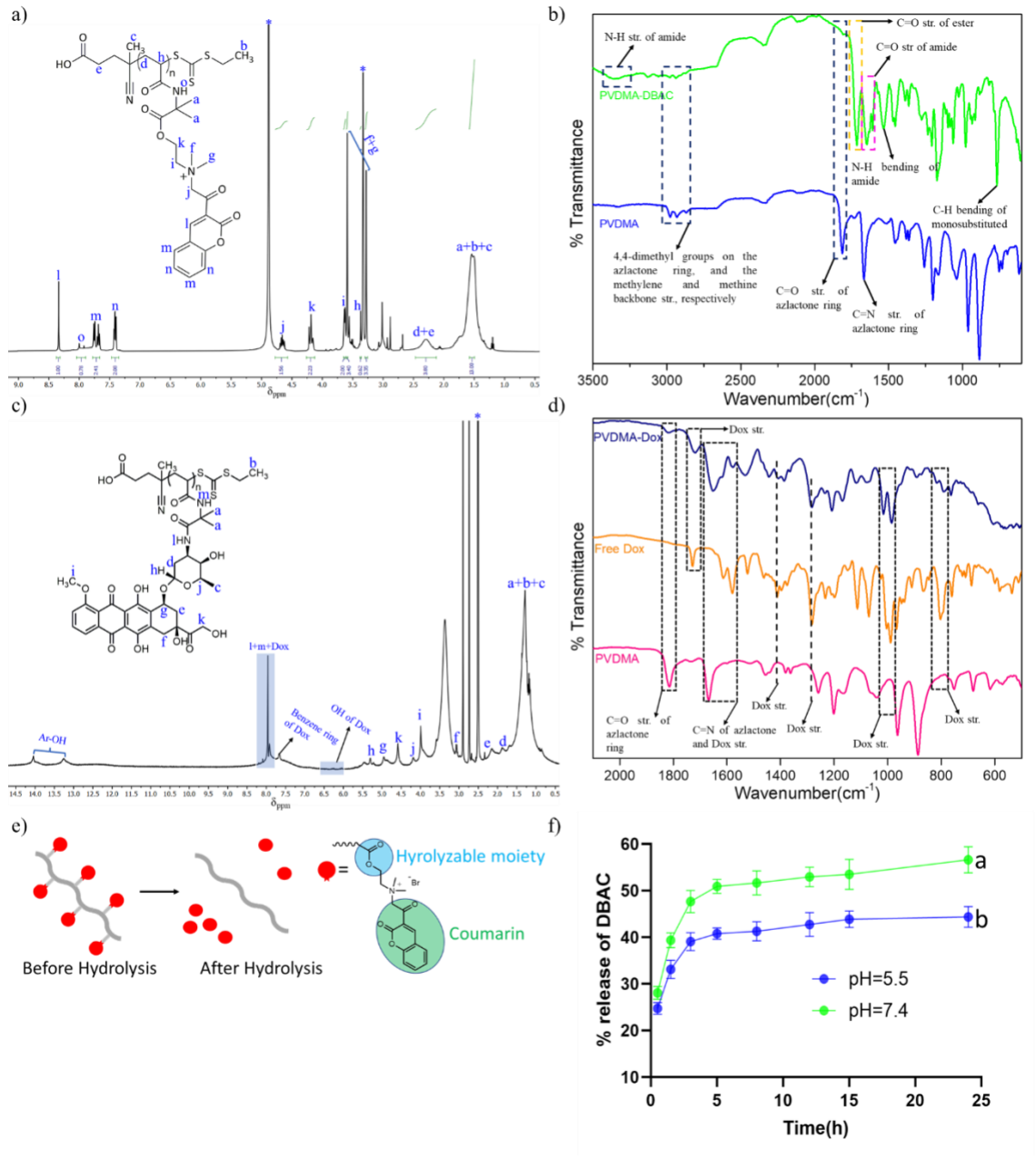

Figure 1. Post-polymerization modification of PVDMA with DBAC and doxorubicin. a) ^{1}H-NMR spectra of DBAC-modified PVDMA polymer in MeOD, (*) solvent peak, b) FTIR spectrum of homopolymer PVDMA, DBAC-modified PVDMA, c) ^{1}H-NMR spectra of doxorubicin-modified PVDMA polymer in DMSO-d6, (*) solvent peak, d) FTIR spectrum of homopolymer PVDMA, free doxorubicin, and doxorubicin-modified PVDMA polymer, e) Schematic of DBAC hydrolysis and release from DBAC-modified PVDMA, f) *In-vitro* release profile of DBAC from DBAC-PVDMA polymers at pH values of 5.5 and 7.4. Data are

expressed as mean ± SD (n =3) and analyzed by Student's t-test: Bars with different letters indicate significant ($P < 0.05$) difference between the pH's.

3.3. Drug release kinetics of DBAC from DBAC-modified PVDMA

We wanted to show that the small molecule DBAC could be liberated from DBAC-modified PVDMA (DBAC-PVDMA) via hydrolysis of ester linkages between DBAC and PVDMA (**Figure 1e**). In order to study the release of DBAC from PVDMA, we dialyzed DBAC-PVDMA against various pH solutions (5.5 and 7.4) at 37 °C and monitored the absorbance of DBAC (316 nm) in supernatants collected from dialysis baths via UV-Vis spectroscopy (**Figure S6**). At 0.5 h, the release of DBAC was observed to be 28% and 25% for pHs 7.4 and 5.5, respectively. The DBAC release rate followed a similar trend up to 5 h. After 5 h, the rate of release of DBAC reached a plateau, while it increased very slowly for both pH 5.5 and 7.4. In between pHs 5.5 and 7.4, the DBAC release rate was comparatively faster at pH 7.4, suggesting that the ester hydrolysis of DBAC-PVDMA (and subsequent release of DBAC) is accelerated at higher pH (**Figure 1f**). ^{1}H-NMR spectra of the DBAC-PVDMA before and after hydrolysis are shown in **Figure S7** and **Figure S8,** respectively. These spectra show that the PVDMA polymer is 100% substituted by DBAC based on the ratio of aromatic protons at ~8.3 ppm to azlactone methyl peaks at ~1.3 ppm. Moreover, the disappearance of the coumarin aromatic moieties (8.3-8.0 ppm) from the polymer backbone after 24 h of incubation in pH 7.4 buffer indicates complete hydrolysis of the ester linkage, which agrees with previous observations of the hydrolysis rate of responsive polymers with carboxylate moieties.[33-36]

3.4. Biocompatibility of DBAC-PVDMA polymer-drug conjugates

Having shown the versatility of PVDMA to form a variety of drug delivery constructs, we next moved to demonstrate the biocompatibility, cell trafficking, and biodistribution of PVDMA

using DBAC-PVDMA as a representative polymer-drug conjugate. DBAC-PVDMA was chosen to move forward because of its high water solubility and the exciting potential of coumarin-based drugs in a variety of pathological settings.[37, 38] The cytotoxicity of DBAC-PVDMA was assessed by measuring the cell viability of multiple cell lines (HeLa and HEK-293) after incubation with the polymers. For concentrations of DBAC-PVDMA up to 330 μg/mL, HeLa and HEK-293 cell lines show viability above 75% after 24 h (**Figure 2a-b**), indicating negligible acute cytotoxicity of the DBAC-PVDMA in cell culture.

3.5. Functionalization of PVDMA polymer with both DBAC and tetramethyl rhodamine cadaverine (TMR)

To synthesize fluorescently-labeled DBAC-PVDMA polymer for cell trafficking studies, we utilized DBAC and TMR reagents to modify the azlactone ring of PVDMA (P3) at a stoichiometric ratio of 99.5:0.5 DBAC:TMR (**Figure 2c**). We checked the ^{1}H-NMR (**Figure S9**) and FTIR (**Figure S10**) spectra to validate the synthetic pathway. ^{1}H-NMR indicated new peaks arising at 7.92-7.89 ppm and 7.47-7.44 ppm when TMR is attached to the azlactone ring of PVDMA. Additionally, the C=O stretching frequency of the azlactone ring at 1810 cm^{-1} completely disappeared after the reaction with DBAC and TMR. Moreover, a peak associated with the ring vibration of TMR appeared at 701 cm^{-1}, confirming the ring opening reaction of the PVDMA polymer with DBAC and TMR was successful to produce DBAC-TMR-PVDMA.

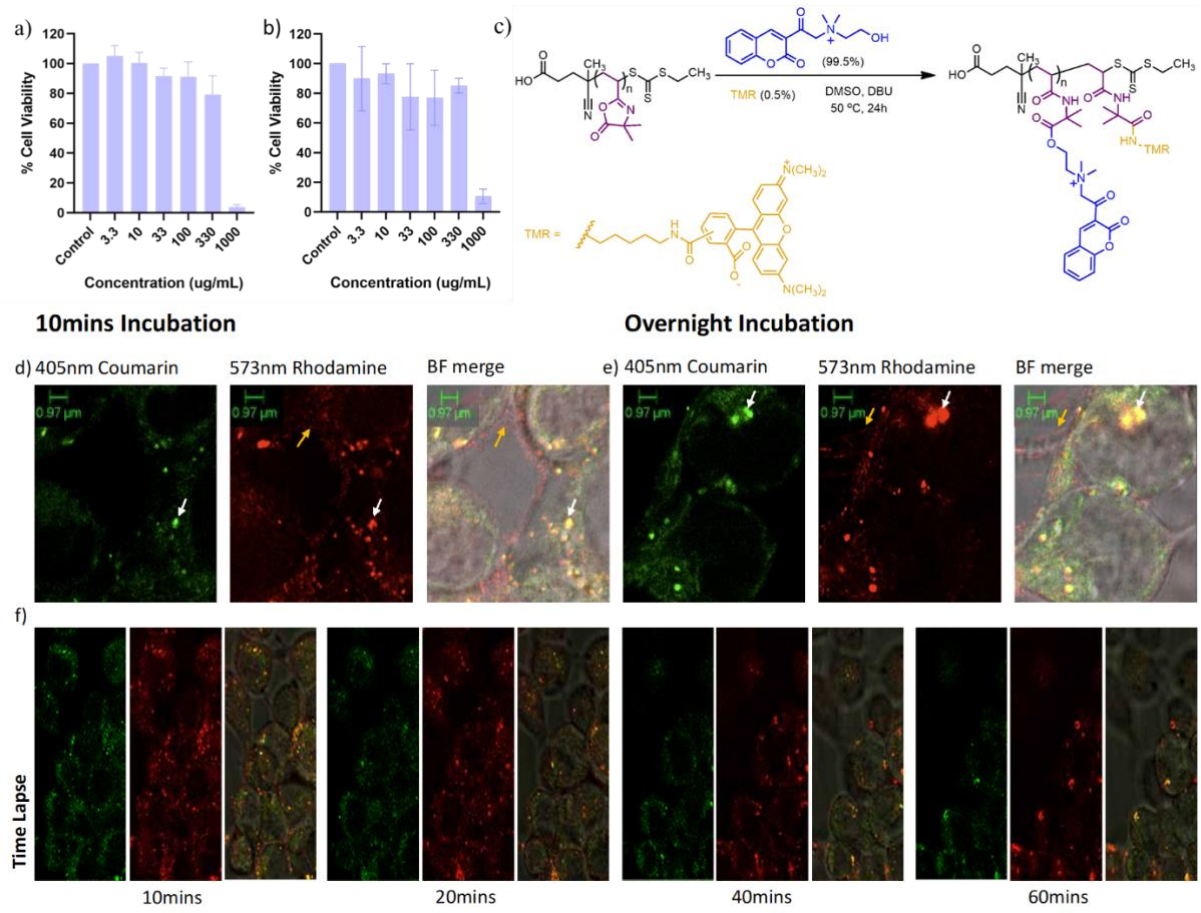

Figure 2. Biocompatibility and cell uptake of DBAC-PVDMA polymers. (a) Cell viability of HeLa cells after incubation with varying concentrations of DBAC-PVDMA (P3) for 24 h (Data represent mean ± s.d., n=4), (b) Cell viability of HEK-293 cells after incubation with different concentrations of DBAC-PVDMA for 24 h (Data represent mean ± s.d., n=4), c) Schematic synthesis diagram of fluorescently-labeled PVDMA polymer (DBAC-TMR-PVDMA), confocal microscopy images of DBAC-TMR-PVDMA in HEK-293 cells d) upon 10 min treatment, e) upon overnight incubation, and f) time-lapse following 10 min treatment.

3.6. Uptake and subcellular distribution of DBAC-TMR-PVDMA polymers

We investigated the intracellular trafficking of DBAC-TMR-PVDMA polymers using super-resolution confocal microscopy of HEK-293 cells, where PVDMA was monitored fluorescently by the irreversible attachment of TMR (*i.e.,* rhodamine derivative) to the polymer

backbone. We began with a pulsed treatment approach where cells were incubated with DBAC-TMR-PVDMA (PVDMA modified with 99.5% DBAC and 0.5% TMR feed ratio) for 10 mins, followed by removal of treatment media and imaging. We observed clear and prominent accumulation of both DBAC and TMR within lysosomes after 10 mins of treatment, indicating colocalization at these early time points (**Figure 2d**). Moreover, we observed minimal interaction of the DBAC-TMR-PVDMA polymers with cell or endolysosomal membranes, suggesting that the polymers maintained water solubility in the cellular environment and were inert to the lipid bilayers of the cell. Next, we investigated the distribution of DBAC-TMR-PVDMA polymer within cells following overnight incubation (*i.e.,* with prolonged exposure to the polymer). Again, we observed an apparent accumulation of both DBAC and TMR within the lysosomes of the cells (**Figure 2e**). However, in the case of overnight incubation, we also began to observe clear cytosolic distribution of the DBAC. This cytosolic distribution was not apparent for TMR from the polymer, suggesting that DBAC was intracellularly liberated from the polymer backbone. Based on the early accumulation of DBAC and TMR within lysosomes of the cells, we anticipate that cleavage of DBAC from the polymer backbone takes place within the lysosomal compartment, followed by diffusion of liberated DBAC into the cytosol. Finally, we pulsed cells with 10 mins of treatment followed by time-lapse imaging for 60 mins after treatment. Time-lapse images again revealed rapid intracellular accumulation of DBAC-TMR-PVDMA with punctate staining that indicated lysosomal colocalization (**Figure 2f**). Additionally, we observed a considerable loss of signal from 10 mins post-treatment to 60 mins post-treatment, which indicates degradation and/or release of the polymers from the cells over time.

To investigate this disparate trafficking of DBAC and the PVDMA polymers (labeled with TMR) further, we performed colocalization experiments after overnight incubation with HEK-293 cells. In addition to monitoring DBAC and TMR fluorescence, we labeled lysosomes

using LysoTracker Green and quantified the colocalization of DBAC, TMR, and LysoTracker (**Figure 3a-c**). As expected, we observed high colocalization of TMR (*i.e.,* polymer) and LysoTracker, with a Pearson's Correlation Coefficient of ~0.8 (**Figure 3d**). DBAC colocalized with lysosomes to a significantly lesser degree, with a 25% reduction in LysoTracker colocalization compared to TMR and Lysotracker. DBAC and TMR colocalization was further reduced, with a Pearson's Correlation Coefficient of less than 0.6. This further supports the notion that DBAC diffuses into the cytosol following its liberation from PVDMA within the lysosomes of the cell.

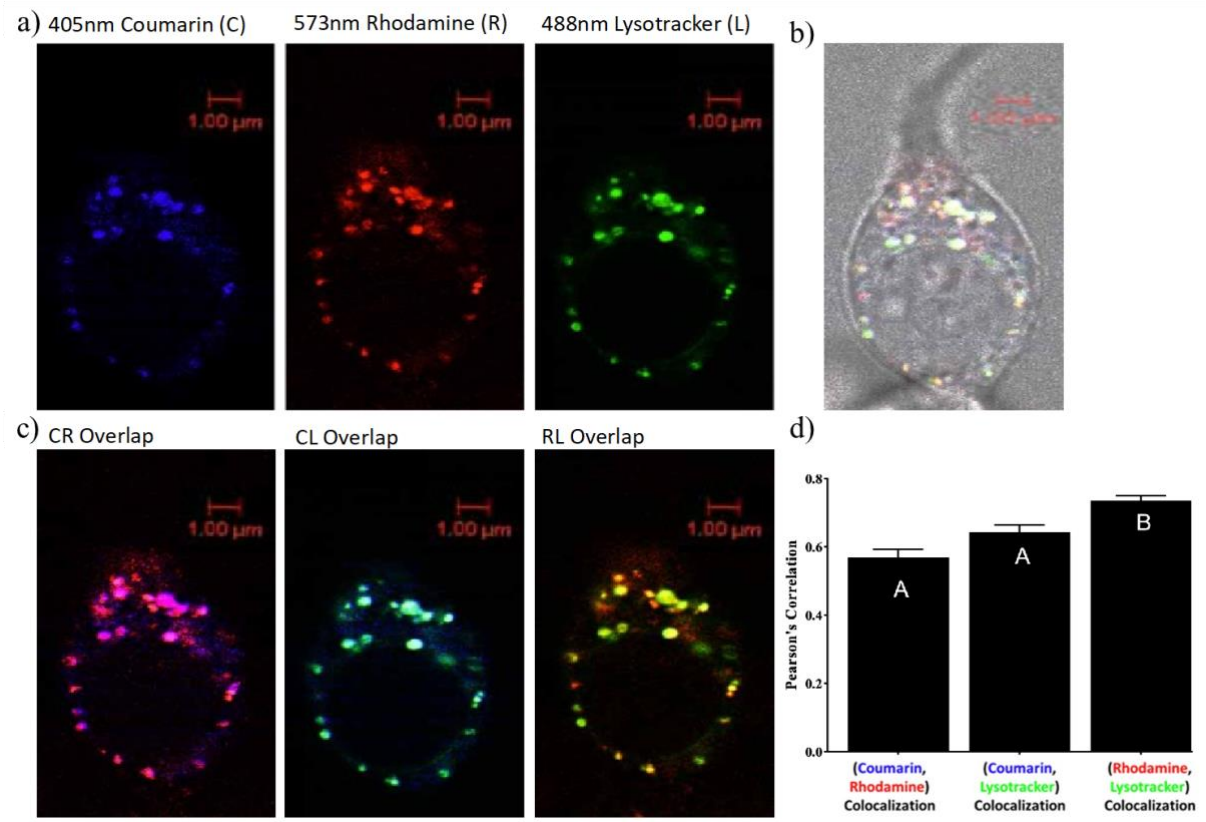

Figure 3. Subcellular colocalization of DBAC and TMR-PVDMA polymer. (a) Fluorescence imaging showing the distribution of DBAC (C), TMR (R), and LysoTracker Green (L) dyes in HEK-293 cells. (b) Fluorescence imaging showing the overlap of all three dyes in HEK-293 cells. DBAC, TMR, and LysoTracker Green dyes, (c) Fluorescence imaging showing the overlap between 2 dyes in HEK-293 cells. Overlap of DBAC and TMR (CR),

DBAC and LysoTracker Green (CL), and TMR and LysoTracker Green (RL) dyes, respectively. (d) Pearson's correlation graph showing the colocalization relationship between two dyes (left-to-right: CR, CL, and RL). ANOVA followed by Tukey's test where different letters indicate statistical significance ($P < 0.05$).

3.7. Pharmacokinetics and biodistribution of DBAC-TMR-PVDMA polymers

We sought to establish the pharmacokinetics and biodistribution of DBAC-TMR-PVDMA polymers since PVDMA-based polymers have broad potential utility for drug delivery but have not been validated to date *in vivo*. Moreover, we investigated the delivery of DBAC-TMR-PVDMA (TMR was included for fluorescent quantification of polymer) by both the oral and intravenous delivery routes to establish the potential for delivery of DBAC-PVDMA polymer-drug conjugates via each of these major delivery routes. Upon IV administration at 10 mg/kg to CD-1 mice, DBAC-TMR-PVDMA polymer persisted well within the plasma with a circulation half-life ($t_{1/2}$) of 2.45±0.98 hrs and area under the curve (AUC) of 27,491±6563 ng*h/mL (**Figure 4a** and **Tables S2-3**). Interestingly, we saw relatively low exposure of the DBAC-TMR-PVDMA polymer within the lungs, spleen, and heart (AUCs of 599±105, 302±14.9, and 863±143 ng*h/g, respectively), while we observed high exposure in the liver (AUC = 9,261±770 ng*h/g) (**Figure 4b-e** and **Tables S2-3**). We also saw high exposure of DBAC-TMR-PVDMA within the kidneys after IV administration (AUC = 9,059±2274 ng*h/g) (**Figure 4f**). Moreover, the concentration of DBAC-TMR-PVDMA in the kidneys steadily increased over time, suggesting that we were observing renal clearance and that DBAC-TMR-PVDMA was accumulating within the kidneys. Consequently, the time of maximum concentration (T_{max}) in the kidneys was substantially delayed compared to other compartments (~8 hrs in kidneys as opposed to < 1 hr in other compartments).

Next, we investigated the biodistribution of DBAC-TMR-PVDMA polymers after oral administration in CD-1 mice. Unsurprisingly, oral administration of DBAC-TMR-PVDMA led to very high exposure in the gastrointestinal (GI) tract (**Figure 5a**). The terminal half-life ($t_{1/2}$) in the GI tract after ingestion of 10 mg/kg DBAC-TMR-PVDMA was 6.97 ± 1.03 h. Moreover, the AUC of the drug in the GI tract was 95,643±1023 ng*h/g after oral administration, which was 5.15x greater than after IV administration (18,544±156 ng*h/g). Interestingly, we found minimal absorption of the DBAC-TMR-PVDMA polymers into the systemic circulation and other organs (**Figures 5b-f**). Indeed, the AUC of DBAC-TMR-PVDMA in all other compartments other than the GI tract was substantially lower via the oral route as compared to IV administration, and negligible drug concentrations were measured in these compartments beyond 1 hr post-administration (**Tables S2-3**).

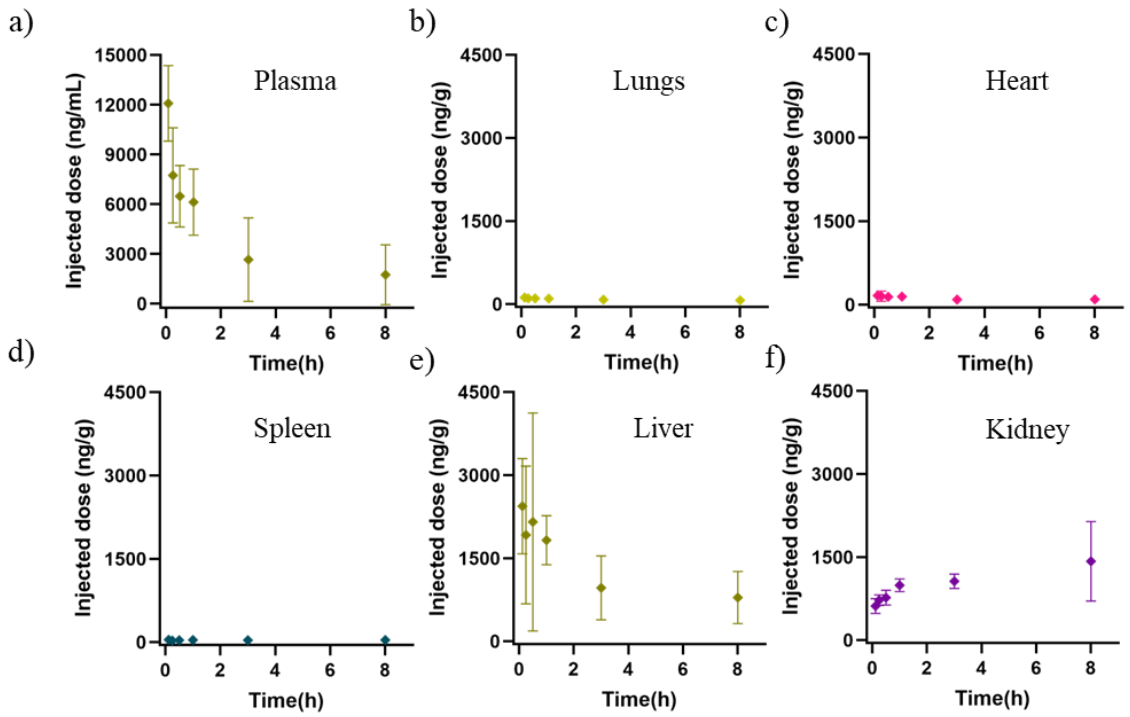

Figure 4. IV Injection of DBAC-TMR-PVDMA extends DBAC circulation and drives kidney accumulation. Pharmacokinetics of DBAC-TMR-PVDMA polymers in (a) plasma, (b) lungs, (c) heart, (d) spleen, (e) liver, and (f) kidney after i.v. injection. (Data represent mean ± s.d., n=3 at each time point)

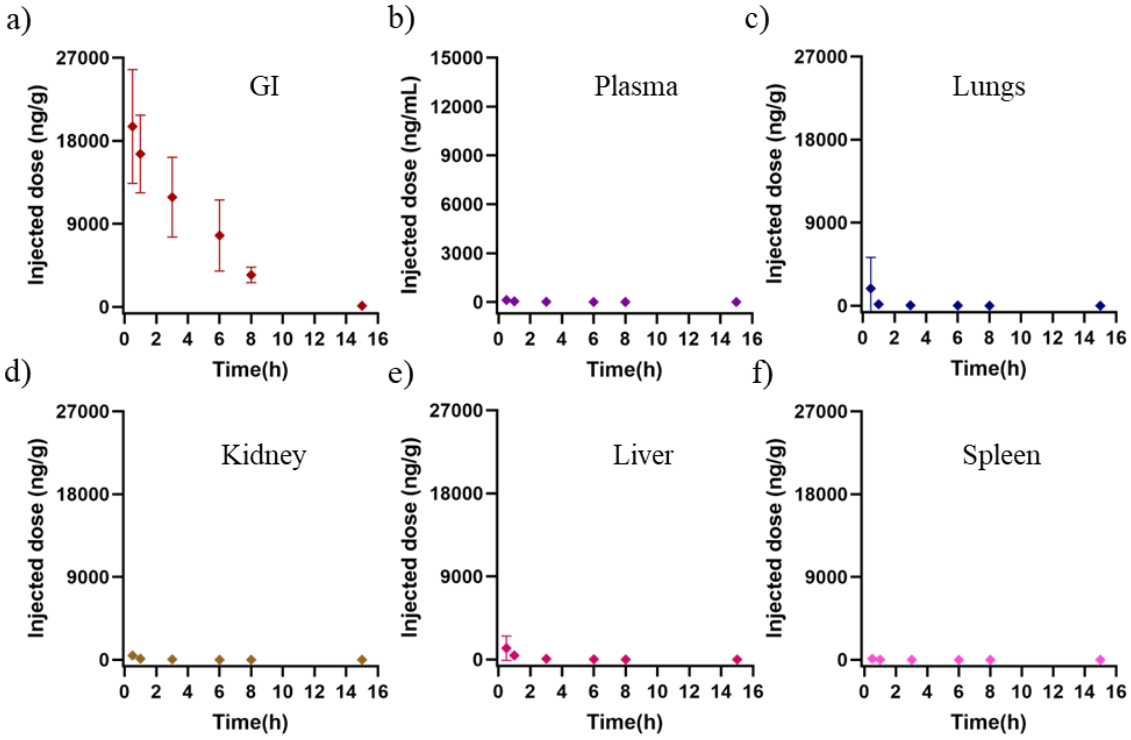

Figure 5. Oral administration of DBAC-TMR-PVDMA drives high accumulation in the GI tract with limited systemic absorption. Pharmacokinetics of DBAC-TMR-PVDMA polymers in the (a) GI tract, (b) plasma, (c) lungs, (d) kidney, (e) liver, and (f) spleen after oral administration. (Data represent mean ± s.d., n=3 at each time point)

3.8. *In Vivo* Biocompatibility of DBAC-PVDMA after Intravenous Administration

We next investigated the biocompatibility of intravenously administered DBAC-PVDMA polymer-drug conjugates at multiple doses. Healthy, immune-competent CD-1 mice injected intravenously with 10 or 33.3 mg/kg showed no variation in body weight when monitored for two weeks after injection (**Figure 6a**). Additionally, we intravenously injected 100 mg/kg DBAC-PVDMA, but acute toxicity was observed in the first two animals injected. Therefore, we determined that the maximum tolerated dose (MTD) for DBAC-PVDMA lies between 33.3 and 100 mg/kg. Next, we assessed organ weights, blood chemistry parameters, and organ

histopathology in mice that had received 10 and 33.3 mg/kg DBAC-PVDMA intravenously. As with overall animal weight, we observed no significant change in the weights of any major organs assessed (heart, lungs, kidney, liver, and spleen) at either dose of DBAC-PVDMA (**Tables S4-5**). The serum markers of the liver (ALP, AST, and ALT) and kidney (BUN) function all showed no increase from baseline with DBAC-PVDMA treatment (**Figure 6b-e**), indicating no toxicity of the polymer-drug conjugates to the liver or kidneys. Interestingly, we observed increased serum creatine kinase levels in animals treated at the highest dose (33.3 mg/kg) DBAC-PVDMA (**Table S6**), suggesting some tissue/skeletal muscle damage in these animals. Lastly, histopathology of the major organs further confirmed no gross toxicity to the major organs was experienced by the animals after treatment with the 10 mg/kg dose of DBAC-PVDMA (**Figure 6f**). Moreover, the histopathology corroborated our observation of elevated creatine kinase (i.e., skeletal muscle damage) in the plasma because gross toxicity to the heart and kidney could also be observed clearly in the histopathology sections. Therefore, we determined that 10 mg/kg DBAC-PVDMA would be the ideal dose to move forward for anti-tumor studies.

3.9.Tumor targeting and anti-tumor efficacy of DBAC-PVDMA

Because of the extended circulation and high biocompatibility of DBAC-PVDMA at 10 mg/kg intravenous dose, we concluded by assessing the tumor targeting and anti-tumor efficacy of DBAC-PVDMA in a model of triple negative breast cancer (TNBC). Fluorescent DBAC-TMR-PVDMA polymer-drug conjugates accumulated efficiently in 4T1 orthotopic breast tumor xenografts after intravenous injection, displaying almost 2-fold higher signal in tumors as opposed to the liver and equivalent signal to the kidneys (**Figures 7a-b**). We observed negligible accumulation of the DBAC-TMR-PVDMA in the spleen, lungs, or heart, matching our initial observation in non-tumor-bearing mice. Since we observed high levels of DBAC-

TMR-PVDMA in tumors and coumarins with a similar structure to DBAC have been reported to have anti-cancer properties,[39,40] we next assessed the anti-tumor efficacy of DBAC-PVDMA in the 4T1 model of TNBC. After 4T1 orthotopic xenografts reached 100 mm^3, we treated mice once weekly (*i.v.*) with either saline, DBAC-PVDMA (10 mg/kg), or DBAC at an equivalent dose. Treatment with DBAC alone showed some modest anti-tumor efficacy from days 9-18, which eventually subsided by day 21 (**Figure 7d**). However, DBAC-PVDMA exhibited rapid and sustained anti-tumor efficacy, *i.e.,* DBAC-PVDMA treated animals had delayed tumor growth as early as six days post-treatment, which was sustained to the end of the study (**Figures 7d-e**).

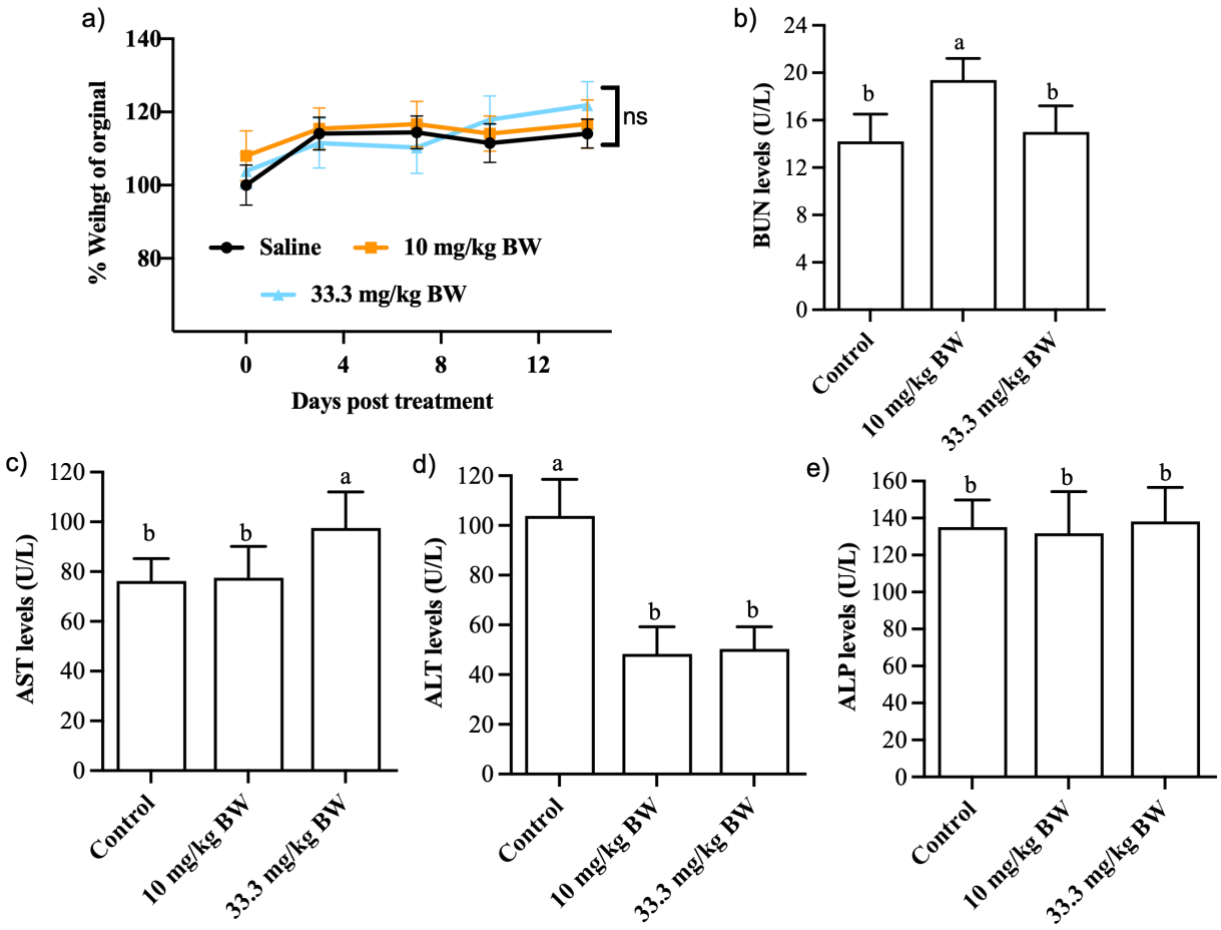

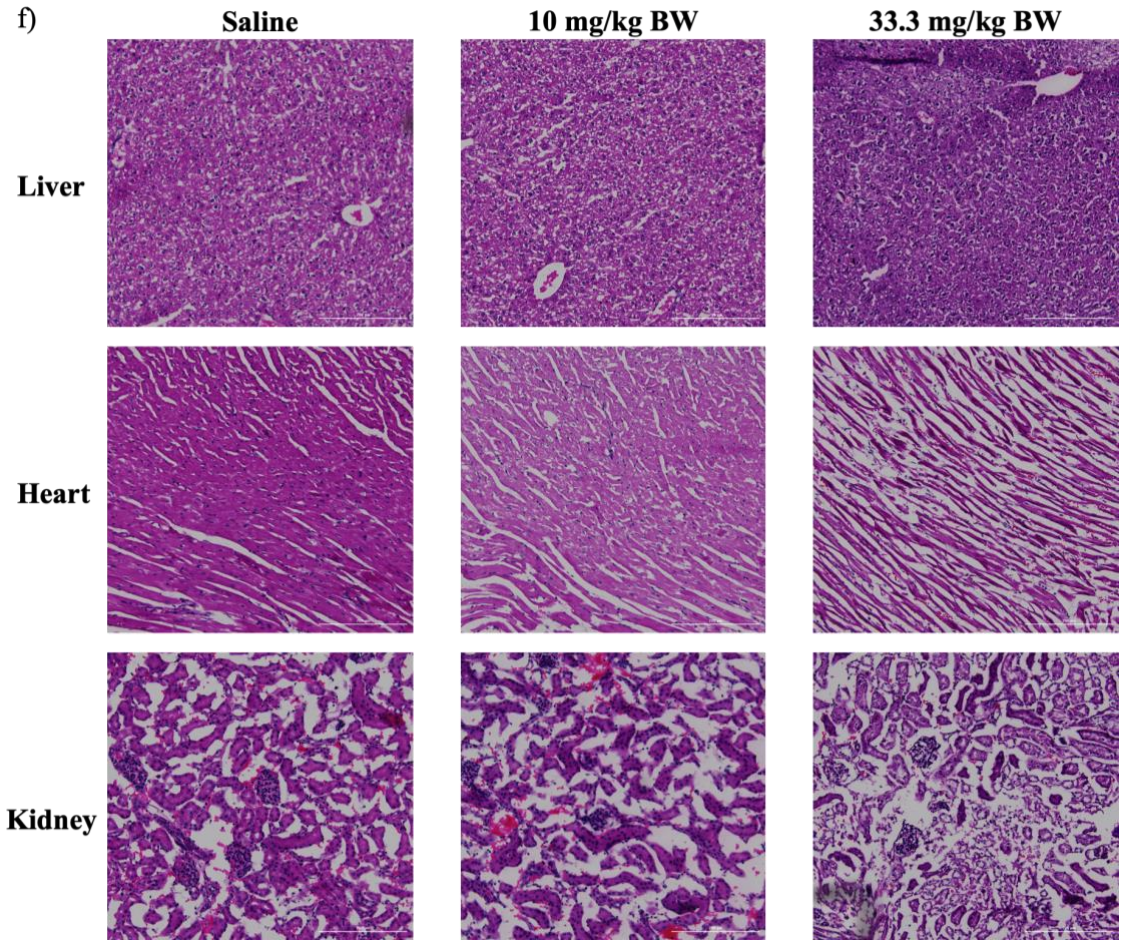

Figure 6. Acute biocompatibility analysis of DBAC-PVDMA after intravenous administration. (a) Body mass of Balb/C mice over time following intravenous injection of saline or DBAC-PVDMA at 10 and 33.3 mg/kg (n = 4). Serum levels of (b) BUN (c) AST (d) ALT, and (e) ALP following intravenous injection of saline or DBAC-PVDMA at 10 and 33.3 mg/kg (n = 4). (f) Representative histopathology images of major organs (liver, heart, and kidneys) following intravenous injection of saline or DBAC-PVDMA (Scale Bar = 200 μm). Data are expressed as mean ± SD (n =4) and analyzed by one-way ANOVA followed by Tukey's test: Bars with different letters indicate significant ($P< 0.05$) difference between the group. Changes in the treatment are represented with respect to the control.

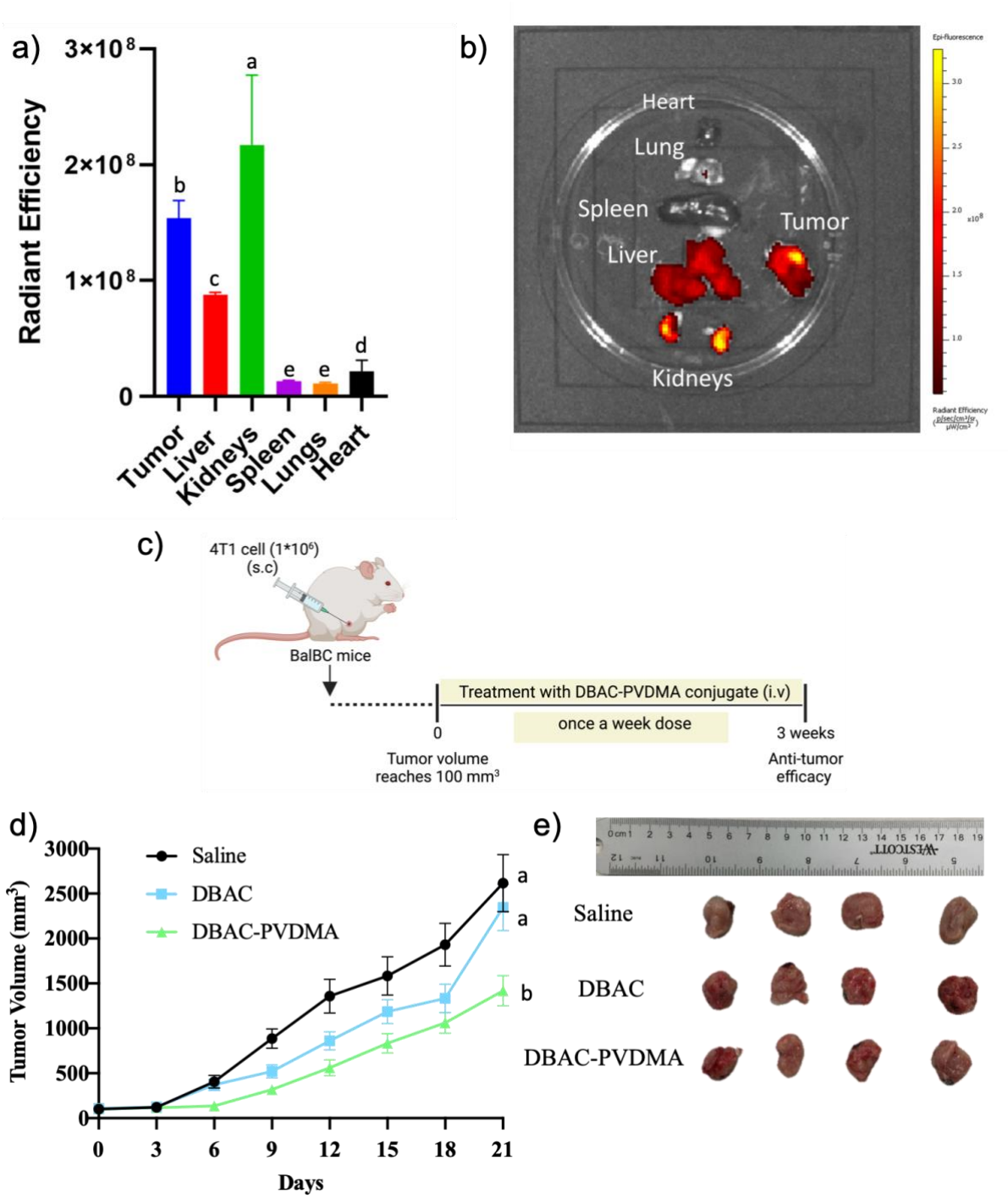

Figure 7. DBAC-PVDMA conjugates exhibit efficient tumor accumulation and anti-tumor efficacy in TNBC xenografts. (a) Quantification of DBAC-TMR-PVDMA levels in major organs and tumor 24 hours following intravenous administration at 10 mg/kg dose (n = 4). (b) Representative IVIS image of DBAC-TMR-PVDMA accumulation in major organs and tumor. (c) Treatment protocol for anti-tumor efficacy study in 4T1 orthotopic mammary

xenografts. (d) Tumor growth curves for saline, DBAC-PVDMA (10 mg/kg), and DBAC (equivalent dose) treatment of 4T1 tumor-bearing mice (n = 4). (e) Image of tumor sizes at study endpoint (n = 4). Data are expressed as mean ± SD (n =4) and analyzed by one-way ANOVA followed by Tukey's test: Bars with different letters indicate significant ($P< 0.05$) difference between the group. Changes in the treatment are represented with respect to the control.

Importantly, this is one of the only reports utilizing PVDMA as a reactive scaffold to form polymer-drug conjugates with small molecule drugs.[5,26] In this study, we demonstrated that DBAC-PVDMA polymer was readily soluble in water, likely due to the incorporation of the tertiary amine of DMAE in the final structure of the conjugate. Since the water solubility of PVDMA is low compared to other hydrophilic polymers utilized for polymer-drug conjugates in the past, this approach could improve the applicability of PVDMA for producing a range of polymer-drug conjugates in the future. Moreover, this approach could be adapted to a range of other hydrophobic drugs in order to produce more hydrophilic PVDMA-based polymer-drug conjugates with improved bioavailability. Since PVDMA had never been assessed *in vivo*, we checked the biodistribution of DBAC-TMR-PVDMA polymers upon IV and oral administration in CD-1 mice. When administered through the IV route, DBAC-TMR-PVDMA persisted well within the plasma and had relatively low exposure in the lungs, spleen, and heart. While we observed high exposure of DBAC-TMR-PVDMA in the liver and kidneys, as expected, it was intriguing to see the steady accumulation and retention of DBAC-TMR-PVDMA in the kidneys over time. It is, therefore, exciting to speculate that PVDMA could be used for targeted drug delivery to the kidneys in future applications. However, more work is needed to confirm the exact location within the kidneys which is being targeted and to confirm that increased renal retention does not lead to any long-term toxicities.

Further, we studied the biodistribution of DBAC-TMR-PVDMA polymers after oral administration in CD-1 mice. Unsurprisingly, we observed that the ingestion of DBAC-TMR-PVDMA led to very high exposure in the gastrointestinal (GI) tract compared to other organs. However, it was interesting to see that systemic exposure of DBAC-TMR-PVDMA remained very low over time, suggesting that DBAC-TMR-PVDMA polymers could remain sequestered within the GI tract and prevent systemic absorption of the drug conjugated to PVDMA. This could be a promising approach to achieve highly-selective GI delivery of compounds that cause toxicities when absorbed systemically. Moreover, this approach pairs well with the base-catalyzed nature of drug release from PVDMA (**Figure 1f**) since slightly elevated pHs in the GI tract will further enable targeted drug release at this site.

In addition to showing the utility of PVDMA as a generic polymer template for drug modification, DBAC-modified PVDMAs could also have strong therapeutic potential. Many coumarin derivatives (similar to the BAC used in these studies) have desirable pharmacological properties, including antiviral, antiproliferative, antioxidant, anticoagulant, anti-HIV, and anti-cancer activities.[39, 40] These coumarins have a straightforward structure, and because of their versatility, they are used for a wide range of applications,[41] including in the cosmetic,[42] pharmaceutical,[43] food,[44] and fragrance industries.[45] However, many derivatives in this class of molecules with wide-ranging physicochemical properties have limited utility because of their poor water solubility and bioavailability. To overcome these issues, we conjugated coumarin derivatives with PVDMA as a novel polymer-drug conjugate synthesis technique. The resulting DBAC-PVDMA displayed high biocompatibility, tumor targeting, and anti-tumor efficacy in a murine model of TNBC. Though simple coumarins such as the DBAC utilized here have been shown to exhibit anti-cancer properties,[36,37] many other compounds based on coumarin derivatives are currently in development as well. It will be exciting to investigate further the anti-tumor efficacy of other coumarin derivatives in future work, using

PVDMA as a modular platform to attach and deliver these compounds to tumors with high bioavailability.

4. CONCLUSIONS

In summary, poly(2-vinyl-4,4-dimethyl azlactone) (PVDMA) is an efficient reactive tool for post-polymerization modification with various small molecule drugs and biologics. We demonstrate the versatile nature of PVDMA scaffolds by modifying them with a coumarin-derivative (DBAC), doxorubicin, and camptothecin. Next, we depicted the controlled release of a model drug (DBAC) from the PVDMA backbone. We have illustrated the intracellular trafficking of a PVDMA derivative for the first time and observed that DBACs are liberated from the polymer intracellularly for cytosolic accumulation. Importantly, we investigated the pharmacokinetics, biodistribution, and anti-tumor efficacy of a PVDMA-based polymer for the first time and showed distinct accumulation patterns depending on the route of administration (*i.e.,* IV vs. oral). The IV and oral routes of administration of DBAC-modified PVDMA could be useful for targeted drug delivery to the kidneys and GI tract, respectively. We also showed that DBAC-modified PVDMA localizes to orthotopic tumor xenografts efficiently after IV administration and inhibits tumor growth of 4T1 tumors. This work opens the door to using PVDMA as a versatile drug delivery template with wide-ranging applications, including the targeted delivery and controlled release of coumarin-based compounds, chemotherapeutics, and other small molecule drugs with poor bioavailability.

SUPPORTING INFORMATION

Additional experimental details, materials, and methods, including characterization techniques, chemical characterization data, and tables of biological data such as pharmacokinetic parameters

ACKNOWLEDGEMENTS

Research reported in this publication was supported by an Institutional Development Award (IDeA) from the National Institute of General Medical Sciences of the National Institutes of Health under award number P20GM103460. This material is based upon work supported by the National Science Foundation under Grant CAREER 2141666. This material is based upon work supported by the American Cancer Society under Grant RSG-21-114-01-MM. The authors would like to thank the University of Mississippi's Biochemistry and Chemistry department for their FTIR facilities. The authors thank the University of Mississippi's Center of Biomedical Research Excellence in Natural Products Neuroscience (COBRE-NPN) for support with animal handling and pharmacokinetics analysis.

REFERENCES

1. N.K. Boaen, M.A. Hillmyer, Post-polymerization functionalization of polyolefins, Chem. Soc. Rev. 34(3) (2005) 267-275, https://doi.org/10.1039/B311405H.

2. M.A. Gauthier, M.I. Gibson, H.A. Klok, Synthesis of functional polymers by post-polymerization modification, Angew. Chem. Int. Ed. 48(1) (2009) 48-58, https://doi.org/10.1002/anie.200801951.

3. E. Pedone, X. Li, N. Koseva, O. Alpar, S. Brocchini, An information rich biomedical polymer library, J Mater. Chem. 13(11) (2003) 2825-2837, https://doi.org/10.1039/B306857A.

4. S.Y. Wong, N. Sood, D. Putnam, Combinatorial evaluation of cations, pH-sensitive and hydrophobic moieties for polymeric vector design, Mol. Ther. 17(3) (2009) 480-490, https://doi.org/10.1038/mt.2008.293.

5. M.E. Buck, D.M. Lynn, Azlactone-functionalized polymers as reactive platforms for the design of advanced materials: Progress in the last ten years, Polym Chem. 3(1) (2012) 66-80, https://doi.org/10.1039/C1PY00314C.

6. Y.M. Zayas-Gonzalez, D.M. Lynn, Degradable amine-reactive coatings fabricated by the covalent layer-by-layer assembly of poly (2-vinyl-4, 4-dimethylazlactone) with degradable polyamine building blocks, Biomacromolecules 17(9) (2016) 3067-3075, https://doi.org/10.1021/acs.biomac.6b00975.

7. S.M. Heilmann, J.K. Rasmussen, L.R. Krepski, Chemistry and technology of 2-alkenyl azlactones, J Polym Sci Part A. 39(21) (2001) 3655-3677, https://doi.org/10.1002/pola.10007.

8. D.F. Veber, S.R. Johnson, H.-Y. Cheng, B.R. Smith, K.W. Ward, K.D. Kopple, Molecular properties that influence the oral bioavailability of drug candidates, J Med Chem. 45(12) (2002) 2615-2623, https://doi.org/10.1021/jm020017n.

9. C.C. Lee, J.A. MacKay, J.M.J Fréchet, F.C. Szoka, Designing dendrimers for biological applications, Nat. Biotechnol. 23(12) (2005) 1517-1526, https://doi.org/10.1038/nbt1171.

10. D. Peer, J.M. Karp, S. Hong, O.C. Farokhzad, R. Margalit, R. Langer, Nanocarriers as an emerging platform for cancer therapy, Nat. Nanotechnol. (2020) 61-91, https://doi.org/10.1038/nnano.2007.387.

11. M.E. Davis, Z. Chen, D.M. Shin, Nanoparticle therapeutics: an emerging treatment modality for cancer, Nat. Rev. Drug Discov. 7(9) (2008) 771-782, https://doi.org/10.1038/nrd2614.

12. J. Liu, W. Liu, I. Weitzhandler, J. Bhattacharyya, X. Li, J. Wang, Y. Qi, S. Bhattacharjee, A. Chilkoti, Ring-opening polymerization of prodrugs: a versatile approach to prepare well-defined drug-loaded nanoparticles, Angew. Chem. Int. Ed. 127(3) (2015) 1016-1020, https://doi.org/10.1002/anie.201409293.

13. J. Liu, Y. Pang, J. Bhattacharyya, W. Liu, I. Weitzhandler, X. Li, A. Chilkoti, Developing Precisely Defined Drug-Loaded Nanoparticles by Ring-Opening Polymerization of a Paclitaxel Prodrug, Adv. Healthc. Mater. 5(15) (2016) 1868-1873, https://doi.org/10.1002/adhm.201600230.

14. J. Huang, A. Heise, Stimuli responsive synthetic polypeptides derived from N-carboxyanhydride (NCA) polymerisation, Chem. Soc. Rev. 42(17) (2013) 7373-7390, https://doi.org/10.1039/C3CS60063G.

15. C. Jérôme, P. Lecomte, Recent advances in the synthesis of aliphatic polyesters by ring-opening polymerization, Adv. Drug Delivery Rev. 60(9) (2008) 1056-1076, https://doi.org/10.1016/j.addr.2008.02.008.

16. S. Zhang, J. Zou, F. Zhang, M. Elsabahy, S.E. Felder, J. Zhu, D.J. Pochan, K.L. Wooley, Rapid and versatile construction of diverse and functional nanostructures derived from a polyphosphoester-based biomimetic block copolymer system, J. Am. Chem. Soc. 134(44) (2012) 18467-18474, https://doi.org/10.1021/ja309037m.

17. J. Feng, R.-X. Zhuo, X.-Z. Zhang, Construction of functional aliphatic polycarbonates for biomedical applications, Prog. Polym. Sci. 37(2) (2012) 211-236, https://doi.org/10.1016/j.progpolymsci.2011.07.008.

18. S.M. Heilmann, J.K. Rasmussen, L.R. Krepski, Chemistry and technology of 2-alkenyl azlactones, J. Polym. Sci. Part A: Polym. Chem. 39(21) (2001) 3655-3677, https://doi.org/10.1002/pola.10007.

19. J. Zhang, L.S. Chua, D.M. Lynn, Multilayered thin films that sustain the release of functional DNA under physiological conditions, Langmuir 20(19) (2004) 8015-8021, https://doi.org/10.1021/la048888i.

20. C.M. Jewell, J. Zhang, N.J. Fredin, M.R. Wolff, T.A. Hacker, D.M. Lynn, Release of plasmid DNA from intravascular stents coated with ultrathin multilayered polyelectrolyte films, Biomacromolecules 7(9) (2006) 2483-2491, https://doi.org/10.1021/bm0604808.

21. J. Zhang, D.M. Lynn, Ultrathin multilayered films assembled from “charge-shifting” cationic polymers: extended, long-term release of plasmid DNA from surfaces, Adv. Mater. 19(23) (2007) 4218-4223, https://doi.org/10.1002/adma.200701028.

22. B. Sun, D.M. Lynn, Release of DNA from polyelectrolyte multilayers fabricated using 'charge-shifting'cationic polymers: Tunable temporal control and sequential, multi-agent release, J. Control. Release 148(1) (2010) 91-100, https://doi.org/10.1016/j.jconrel.2010.07.112.

23. B. Sun, X. Liu, M.E. Buck, D.M. Lynn, Azlactone-functionalized polymers as reactive templates for parallel polymer synthesis: synthesis and screening of a small library of cationic polymers in the context of DNA delivery, Chem. Commun. 46(12) (2010) 2016-2018, https://doi.org/10.1039/B921664B.

24. S. Ros, J.S. Freitag, D.M. Smith, H.D.H Stöver, Charge-Shifting Polycations Based on N, N-(dimethylamino) ethyl Acrylate for Improving Cytocompatibility During DNA Delivery, ACS Omega 5(16) (2020) 9114-9122, https://doi.org/10.1021/acsomega.9b03734.

25. J.S. Kim, A.R. Sirois, A.J. Vazquez Cegla, E. Jumai'an, N. Murata, M.E. Buck, S.J. Moore, Protein–Polymer Conjugates Synthesized Using Water-Soluble Azlactone-Functionalized Polymers Enable Receptor-Specific Cellular Uptake toward Targeted Drug Delivery, Bioconjug. Chem. 30(4) (2019) 1220-1231, https://doi.org/10.1021/acs.bioconjchem.9b00155.

26. H.T.T. Duong, Z.M. Kamarudin, R.B. Erlich, Y. Li, M.W. Jones, M. Kavallaris, C. Boyer, T.P. Davis, Intracellular nitric oxide delivery from stable NO-polymeric nanoparticle carriers, Chem. Commun. 49 (2013) 4190-4192, https://doi.org/10.1039/C2CC37181B.

27. J. J. Donohue; D. A. Buttry, Adsorption and micellization influence the electrochemistry of redox surfactants derived from ferrocene. Langmuir 5 (3) (1989) 671-678, https://doi.org/10.1021/la00087a020.

28. M. E. Buck; D. M. Lynn, Functionalization of fibers using azlactone-containing polymers: layer-by-layer fabrication of reactive thin films on the surfaces of hair and cellulose-based materials. ACS Appl. Mater. Interfaces. 2 (5) (2010) 1421-1429, https://doi.org/10.1021/am1000882.

29. V. Toragall, N. Jayapala, S. P. Muthukumar, and B. Vallikanan. "Biodegradable chitosan-sodium alginate-oleic acid nanocarrier promotes bioavailability and target delivery of lutein in rat model with no toxicity." Food chemistry 330 (2020): 127195. https://doi.org/10.1016/j.foodchem.2020.127195.

30. D. Sajan, Y. Erdogdu, R. Reshmy, Ö. Dereli, K.K. Thomas, I.H. Joe, Spectroscopy, DFT-based molecular modeling, NBO analysis and vibrational spectroscopic study of 3-(bromoacetyl) coumarin, Spectrochim. Acta A Mol. Biomol. Spectrosc. 82(1) (2011) 118-125, https://doi.org/10.1016/j.saa.2011.07.013.

31. S. Deshmukh, P.B. Undre, K.L. Pattebahadur, A.G. Mohod, S.S. Patil, P.W. Khirade, Investigation of intermolecular interactions between amide-amine binary mixtures through dielectric relaxation study, Ferroelectrics 519(1) (2017) 23-32, https://doi.org/10.1080/00150193.2017.1362280.

32. Y. Zhu, J.Y. Quek, A.B. Lowe, P.J. Roth, Thermoresponsive (Co) polymers through Post-polymerization Modification of Poly (2-vinyl-4, 4-dimethylazlactone), Macromolecules 46(16) (2013) 6475-6484, https://doi.org/10.1021/ma401096r.

33. P. Van de Wetering, N.J. Zuidam, M.J. Van Steenbergen, O.A.J. Van Der Houwen, W. Underberg, W.E. Hennink, A mechanistic study of the hydrolytic stability of poly (2-(dimethylamino) ethyl methacrylate), Macromolecules 31(23) (1998) 8063-8068, https://doi.org/10.1021/ma980689g.

34. P. Cotanda, D.B. Wright, M. Tyler, R.K. O'Reilly, A comparative study of the stimuli-responsive properties of DMAEA and DMAEMA containing polymers, J. Polym. Sci. Part A: Polym. Chem. 51(16) (2013) 3333-3338, https://doi.org/10.1002/pola.26730.

35. S. Ros, J. Wang, N.A.D. Burke, H.D.H. Stöver, A Mechanistic Study of the Hydrolysis of Poly [N, N-(dimethylamino) ethyl acrylates] as Charge-Shifting Polycations, Macromolecules 53(9) (2020) 3514-3523, https://doi.org/10.1021/acs.macromol.9b02272.

36. Y. Bernhard, O. Sedlacek, J.F.R. Van Guyse, J. Bender, Z. Zhong, B.G. De Geest, R. Hoogenboom, Poly (2-ethyl-2-oxazoline) conjugates with salicylic acid via degradable modular ester linkages, Biomacromolecules 21(8) (2020) 3207-3215, https://doi.org/10.1021/acs.biomac.0c00659.

37. K.N. Venugopala, V. Rashmi, B. Odhav, Review on natural coumarin lead compounds for their pharmacological activity, Biomed Res. Int. 2013 (2013), https://doi.org/10.1155/2013/963248.

38. M.N. Ristić, N.S. Radulović, B.R. Dekić, V.S. Dekić, N.R. Ristić, Z. Stojanović-Radić, Synthesis and spectral characterization of asymmetric azines containing a coumarin moiety: the discovery of new antimicrobial and antioxidant agents, Chem Biodivers 16(1) (2019) e1800486, https://doi.org/10.1002/cbdv.201800486.

39. G. Melagraki, A. Afantitis, O. Igglessi-Markopoulou, A. Detsi, M. Koufaki, C. Kontogiorgis, D.J. Hadjipavlou-Litina, Synthesis and evaluation of the antioxidant and anti-inflammatory activity of novel coumarin-3-aminoamides and their alpha-lipoic acid adducts, Eur. J. Med. Chem. 44(7) (2009) 3020-3026, https://doi.org/10.1016/j.ejmech.2008.12.027.

40. B. Sandhya, D. Giles, V. Mathew, G. Basavarajaswamy, R. Abraham, Synthesis, pharmacological evaluation and docking studies of coumarin derivatives, Eur. J. Med. Chem. 46(9) (2011) 4696-4701, https://doi.org/10.1016/j.ejmech.2011.07.013.

41. M.J. Matos, L. Santana, E. Uriarte, O.A. Abreu, E. Molina, E.G. Yordi, Coumarins—an important class of phytochemicals, IntechOpen 25 (2015) 533-538, https://dx.doi.org/10.5772/59982.

42. C. Stiefel, T. Schubert, G.E. Morlock, Bioprofiling of cosmetics with focus on streamlined coumarin analysis, ACS omega 2(8) (2017) 5242-5250, https://doi.org/10.1021/acsomega.7b00562.

43. X.-M. Peng, G. LV Damu, C.H. Zhou, Current developments of coumarin compounds in medicinal chemistry, Curr Pharm Des 19(21) (2013) 3884-3930.

44. E.F.S. Authority, Coumarin in flavourings and other food ingredients with flavouring properties-Scientific Opinion of the Panel on Food Additives, Flavourings, Processing Aids and Materials in Contact with Food (AFC), EFSA J 6(10) (2008) 793, https://doi.org/10.2903/j.efsa.2008.793.

45. P.M. Boisde, W.C. Meuly and Staff, U.b., Coumarin, In Kirk-Othmer Encyclopedia of Chemical Technology, John Wiley & Sons, Inc (Ed.)., 4 (2014) 1–10, https://doi.org/10.1002/0471238961.0315211302150919.a01.pub2.

For Table of Contents Only

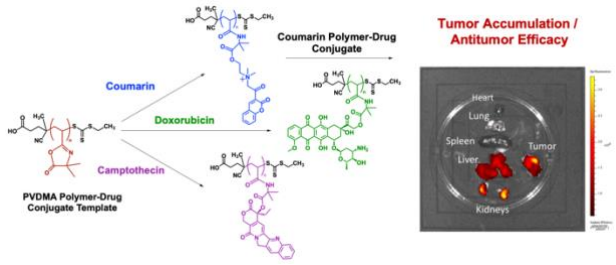
Coumarin
Doxorubicin
Camptothecin
PVDMA Polymer-Drug
Conjugate Template
Coumarin Polymer-Drug
Conjugate

Tumor Accumulation /
Antitumor Efficacy
Heart
Lung
Spleen
Liver
Tumor
Kidneys